Dynamic Reconstruction with Statistical Ray Weighting for C-Arm CT Perfusion Imaging

Michael T. Manhart, Andreas Fieselmann, Yu Deuerling-Zheng, Andreas K. Maier and Markus Kowarschik

***Abstract*—Tissue perfusion measurement using C-arm angiography systems is a novel technique with potential high benefit for catheter-guided treatment of stroke in the interventional suite. However, perfusion C-arm CT (PCCT) is challenging: the slow C-arm rotation speed only allows measuring samples of contrast time attenuation curves (TACs) every 5 – 6 s if reconstruction algorithms for static data are used. Furthermore, the peaks of the tissue TACs typically lie in a range of 5 – 30 HU, thus perfusion imaging is very sensitive to noise. Recently we presented a dynamic, iterative reconstruction (DIR) approach to reconstruct TACs described by a weighted sum of linear spline functions with a regularization based on joint bilateral filtering (JBF). In this work we incorporate statistical ray weighting into the algorithm and show how this helps to improve the reconstructed cerebral blood flow (CBF) maps in a simulation study with a realistic dynamic brain phantom. The Pearson correlation of the CBF maps to ground truth maps increases from 0.85 (FDK), 0.87 (FDK with JBF), and 0.90 (DIR with JBF) to 0.92 (DIR with JBF and ray weighting). The results suggest that the statistical ray weighting approach improves the diagnostic accuracy of PCCT based on DIR.**

I. Introduction

Perfusion CT (PCT) is an important imaging modality for diagnosis in case of an ischemic stroke event. Time attenuation curves (TACs) in tissue and vessels are extracted from a time series of brain volumes acquired after a contrast bolus injection. Perfusion parameter maps calculated from TACs, which represent quantities such as cerebral blood flow (CBF), cerebral blood volume (CBV), and mean transit time (MTT), provide information about the extent of the affected tissue. They can be used to identify potentially salvageable ischemic tissue that may be reperfused by catheter-guided stroke therapy procedures such as intra-arterial thrombolysis. For this purpose the patient is transported to an interventional suite equipped with a C-arm angiography system, where perfusion measurement is not yet available. Perfusion measurement using C-arm systems would allow assessing the perfusion parameters directly before, during and after the interventional procedure and thus help to determine treatment success and endpoint [1]. Current C-arm systems typically require about 4 – 5 s to acquire the X-ray projection images needed to reconstruct one volume and a pause of about 1 s between two successive acquisitions, which limits the temporal sampling of the TACs and makes perfusion C-arm CT (PCCT) challenging. Recently we proposed a new dynamic, iterative reconstruction algorithm with a joint bilateral filter (DIR-JBF) [2] to reconstruct TACs from a PCCT acquisition with increased temporal resolution and improved CNR in the brain tissue compared to standard FDK reconstruction. In this work, we additionally introduce a statistical ray weighting to further improve the reconstructed perfusion maps. We investigate the noise statistics of subtracted projections and introduce a penalized weighted least squares (PWLS) formulation extending the DIR-JBF algorithm to the DIR *maximum a-posteriori* (DIR-MAP) algorithm. The new DIR-MAP algorithm is evaluated using a digital brain phantom and compared to the DIR-JBF algorithm, classical FDK reconstruction and FDK reconstruction followed by denoising with JBF (FDK-JBF).

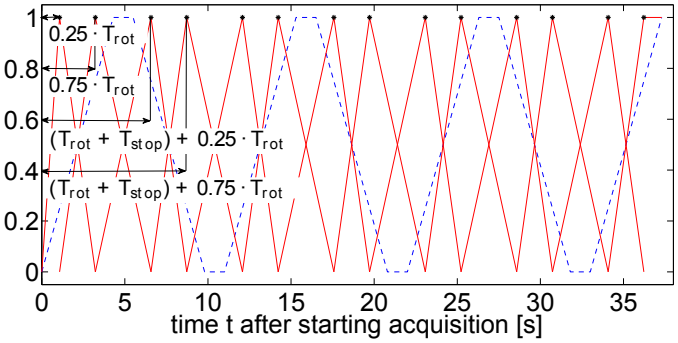

Figure 1. Basis functions for linear interpolation (red, solid) and relative angular C-arm position (blue, dashed).

II. Algorithm

A. Acquisition Protocol

This section describes the C-arm perfusion acquisition protocol used for the simulation study. The parameters are taken from an acquisition protocol available in state-of-the-art C-arm systems (Artis zee, Siemens Healthcare, Germany). Since currently available C-arm systems are not capable of continuous, uni-directional rotations, the C-arm is rotated in a bi-directional manner in forward and backward direction during a perfusion scan. At first one C-arm rotation in forward and one in backward direction acquires mask projection data $\mathbf{p}^{\mathrm{M}}$ (M: mask) with the static anatomical structures. In each rotation 248 projections covering an angular range of 197.6° are acquired. After contrast agent injection the C-arm is rotated $N_{\mathrm{rot}} = 7$ times in bi-directional manner as shown in Figure 1 and acquires the projections $\mathbf{p}^{\mathrm{B}}$ (B: bolus) following the contrast bolus flow. Each rotation takes $T_{\mathrm{rot}} = 4.3\,\mathrm{s}$ with a pause of $T_{\mathrm{stop}} = 1.2\,\mathrm{s}$ between any two of them. After logarithmic

M.T. Manhart, A. Fieselmann and A.K. Maier are with Pattern Recognition Lab, Department of Computer Science, Friedrich-Alexander-Universität Erlangen-Nürnberg, Martensstr. 3, 91058 Erlangen, Germany. Y. Deuerling-Zheng and M. Kowarschik are with Siemens AG, Healthcare Sector, Angiography & Interventional X-Ray Systems, Forchheim, Germany.

Email: michael.manhart@cs.fau.de

pre-processing the pure contrast-enhanced projection data $\mathbf{p}$ is computed by subtracting the mask projections $\mathbf{p}^{\mathrm{M}}$ from the bolus projections $\mathbf{p}^{\mathrm{B}}$.

B. Dynamic Iterative Reconstruction Algorithm

The DIR-JBF algorithm [2] represents the basis method used to reconstruct the contrast time attenuation curves (TACs) inside the volume of interest (VOI) from the dynamic projection data denoted by vector $\mathbf{p} \in \mathcal{R}^N$, which comprehends all rays during the contrast-enhanced acquisition after mask subtraction. Each TAC inside the VOI is described by a weighted sum of asymmetric linear spline functions. The knots of the splines are placed at $0.25 \cdot T_{\mathrm{rot}}$ and $0.75 \cdot T_{\mathrm{rot}}$ of each C-arm rotation (Figure 1). Consider the 4D volume denoted by vector $\mathbf{x}$ describing the TACs sampled at the acquisition time point of each acquired contrast-enhanced C-arm projection. We introduce the matrix $\mathbf{B}$, which interpolates $\mathbf{x}$ from the weights of all basis functions denoted by vector $\mathbf{w}$ such that $\mathbf{x} = \mathbf{B}\mathbf{w}$. The system matrix $\mathbf{A}$ describes the dynamic forward projection $\mathbf{p} \approx \mathbf{A}\mathbf{x}$. The DIR-JBF algorithm reconstructs the basis weights $\mathbf{w}$ from $\mathbf{p}$ by minimizing the least-squares distance between the measured projection data $\mathbf{p}$ and the forward projected estimated 4D volume:

$$\tilde{\mathbf{w}} = \underset{\mathbf{w}}{\operatorname{argmin}} \frac{1}{2} \left\| \mathbf{A}\mathbf{B}\mathbf{w} - \mathbf{p} \right\|_2^2 . \tag{1}$$

This large scale problem can be solved as described in [3] by using a gradient-based iterative procedure based on the Landweber scheme:

$$\mathbf{w}^{k+1} = \mathbf{w}^k + \beta \cdot \mathbf{B}^T \mathbf{A}^T \left(\mathbf{p} - \mathbf{A}\mathbf{B}\mathbf{w}^k \right) . \tag{2}$$

The parameter β controls the step size of the parameter update in each iteration, $\mathbf{AB}$ describes a linear interpolation followed by forward projection and $\mathbf{B}^T\mathbf{A}^T$ represents a weighted backprojection of the error image onto the basis weights. As described in [2] the gradient update step is using a vessel-masked backprojection, where rays intersecting with high contrast vessel structures are only backprojected onto voxels belonging to the vessel structures. The weight vector $\mathbf{w}$ is initialized from FDK reconstructions of the C-arm rotations. Furthermore JBF is used for regularization. JBF is an adapted version of the bilateral filter, where the range similarity image is computed using a guidance image. In the DIR-JBF algorithm the temporal maximum intensity projections of the reconstructed TACs are used as guidance image. We modify the JBF regularization compared to [2]: after FDK initialization $N_{\mathrm{JBF}} = 3$ JBF iterations are applied. During the DIR, JBF is applied once after every three gradient update steps. To show the benefits of the dynamic iterative reconstruction algorithm compared to pure FDK reconstruction followed by JBF the result of the initialization is included in the evaluation. Applying only the initialization step is denoted as the FDK-JBF algorithm.

C. Statistical Ray Weighting

In this section we discuss how we model the noise in the subtracted projection data $\mathbf{p}$ and include a statistical noise model into the DIR-JBF algorithm to extend it to the DIR-MAP algorithm. The number of photons measured at the C-arm detector is considered as a Poisson random process to simulate quantum noise. The number of photons reaching a detector pixel is related to the line integral p by $i = i^{\mathrm{S}} \exp(-p)$, where i^{S} denotes the number of photons emitted at the source. Incorporating quantum noise, the number of actually measured photons is a Poisson random process: $\hat{i} \sim \mathcal{P}(\mu_{\mathrm{P}} = i)$ (P: photons). Since we do tomographic brain imaging we assume a large number of counts; i.e. $i > 1000$. For such large counts a Gaussian process is an excellent approximation of the Poisson process:

$$\hat{i} \sim \mathcal{N}\left(\mu_{\mathrm{P}} = i; \sigma_{\mathrm{P}} = \sqrt{i} \right) .$$

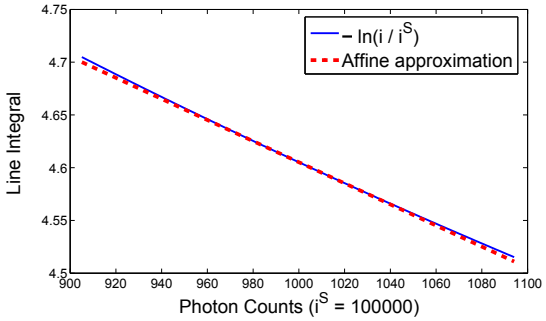

Figure 2. First order Taylor approximation of logarithmic pre-processing around a photon count of $i = 1000$ in the $3\,\sigma_{\mathrm{P}}$ interval of the corresponding Gaussian random process $\hat{i}$ (99.7 % of measurements of 1000 photons will be inside the interval $[1000 - 3\,\sigma_{\mathrm{P}} \quad 1000 + 3\,\sigma_{\mathrm{P}}]$; $\sigma_{\mathrm{P}} = \sqrt{1000}$).

The measured line integrals are also random variables and related to the photon counts by $\hat{p}\left(\hat{i}\right) = -\ln\left(\hat{i}/i^{\mathrm{S}}\right)$. As discussed in [4] for large photon counts we can simplify the logarithmic processing by a first order Taylor series development of $\hat{p}\left(\hat{i}\right)$ around $\mu_{\mathrm{P}} = i$:

$$\begin{aligned} \hat{p}\left(\hat{i}\right) &\approx \hat{p}(i) + \hat{p}'(i)\left(\hat{i} - i\right) \\ &= -\ln\frac{i}{i^{\mathrm{S}}} + \frac{i - \hat{i}}{i}. \end{aligned} \tag{3}$$

Figure 2 shows that the first order development is an appropriate approximation inside the $3\,\sigma_{\mathrm{P}}$ interval of $\hat{i}$. From Equation 3 we see that the logarithmic processing $\hat{p}\left(\hat{i}\right)$ is mainly a scaling with $-1/i$ and shifting with $-\ln\left(i/i^{\mathrm{S}}\right) + 1$. Thus the line integral random variable $\hat{p}$ can also be described as a Gaussian process with mean $\mu_{\mathrm{L}} = \mu_{\mathrm{P}}/i - \ln(i/i_{\mathrm{S}}) + 1 = -\ln(i/i_{\mathrm{S}})$ and variance $\sigma_{\mathrm{L}} = \sigma_{\mathrm{P}}/i$ (L: line integrals):

$$\hat{p} \sim \mathcal{N}\left(\mu_{\mathrm{L}} = -\ln(i/i_{\mathrm{S}}); \sigma_{\mathrm{L}} = 1/\sqrt{i} \right) . \tag{4}$$

Modeling the noise in line integral domain by Gaussian random processes allows to describe the subtraction of the mask measurements from the contrast-enhanced measurements as a subtraction of two independent Gaussian random processes. Thus a mask-subtracted contrast measurement $\hat{p}^{\mathrm{S}} = \left(\hat{p}^{\mathrm{B}} - \hat{p}^{\mathrm{M}}\right)$ (S: subtracted) is again a Gaussian process:

$$\hat{p}^{\mathrm{S}} \sim \mathcal{N}\left(\mu_{\mathrm{L}}^{\mathrm{S}} = p^{\mathrm{B}} - p^{\mathrm{M}}; \sigma_{\mathrm{L}}^{\mathrm{S}} = \sqrt{1/i^{\mathrm{B}} + 1/i^{\mathrm{M}}} \right) . \tag{5}$$

Parameter	FDK	FDK-JBF	DIR-JBF	DIR-MAP
σ_{K}	1.25	0.25	0.25	0.25
σ_{D}		1.5 mm	1.5 mm	1.5 mm
σ_{R0}		0.001	0.001	0.001
σ_{R}		$1.25 \cdot 10^{-4}$	$1.25 \cdot 10^{-4}$	$1.25 \cdot 10^{-4}$
β			3	12
N_{JBF}		3	3	3
N_{DIR}			12	12

σ_{K}: smoothness of FDK filter kernel for initial reconstruction,
σ_{D}: spatial bandwidth of JBF, σ_{R0}: range bandwidth of initial JBF,
σ_{R}: range bandwidth of JBF, β: DIR update step size,
N_{JBF}: number of initial JBF iterations,
N_{DIR}: number of DIR-JBF/DIR-MAP iterations

Table I
PARAMETERS OF ALGORITHMS.

The maximum likelihood (ML) estimation of the weights $\mathbf{w}$ from projection data with Gaussian noise is provided by the corresponding log-likelihood function [5], which combines Equation 1 with the diagonal weighting matrix $\mathbf{D}$ to the squared Mahalanobis distance $\mathcal{D}(\mathbf{w})$:

$$\mathcal{D}(\mathbf{w}) = \frac{1}{2}(\mathbf{ABw} - \mathbf{p})^T \mathbf{D}(\mathbf{ABw} - \mathbf{p}), \qquad (6)$$

where $\mathbf{D} = \mathrm{diag}\left\{1/\left(\sigma^{\mathrm{S}}_{\mathrm{L},1}\right)^2, \ldots, 1/\left(\sigma^{\mathrm{S}}_{\mathrm{L},N}\right)^2\right\}$, with N defined in subsection II-B. Note that in the case of non-subtracted projections the ML estimation would be the same as in well-known statistical reconstruction algorithms [6]. However, our derivation also allows to describe the noise in subtracted projections.

Elad [7] showed that the bilateral filter is related to Bayesian noise removal. Thus we can combine the ML estimate of the weights with a JBF penalty function $\mathcal{R}^{\mathrm{JBF}}(\mathbf{w})$ resulting in the *maximum a-posteriori* (MAP) estimate, which can be formulated as a PWLS problem :

$$\tilde{\mathbf{w}} = \underset{\mathbf{w}}{\mathrm{argmin}}\, \mathcal{D}(\mathbf{w}) + \lambda \mathcal{R}^{\mathrm{JBF}}(\mathbf{w}). \qquad (7)$$

The weights are then updated by the following gradient-based iterative procedure:

$$\mathbf{w}^{k+1} = \mathbf{w}^k + \beta \cdot \mathbf{B}^T \mathbf{A}^T \mathbf{D}\left(\mathbf{p} - \mathbf{ABw}^k\right). \qquad (8)$$

Analogous to the DIR-JBF algorithm, the weights are initialized from FDK reconstructions and filtered $N_{\mathrm{JBF}} = 3$ times after FDK initialization and once after every three gradient update steps. Also vessel masking is applied in the backprojection step. In this work we use the approximation $\mathbf{D} = \mathrm{diag}\left\{\exp\left(-p^{\mathrm{M}}_1\right), \ldots, \exp\left(-p^{\mathrm{M}}_N\right)\right\}$. The contrast attenuation is very small compared to the attenuation of the anatomic structures and thus $\sigma^{\mathrm{S}}_{\mathrm{L},i} \approx \sqrt{2/i^{\mathrm{M}}_i} = \sqrt{2/\left(i^{\mathrm{S}} \exp\left(-p^{\mathrm{M}}_i\right)\right)}$, which results in the above weighting matrix after omitting the constants.

III. MATERIALS & METHODS

We evaluate the different approaches using the realistic digital brain perfusion phantom, which was originally described in [8] and extended for C-arm perfusion imaging in [9]. The phantom is based on segmentation of a human MR brain scan and simulates TACs inside a stroke-affected brain. The phantom is available online [10]. Different regions with reduced blood flow and volume were annotated in the brain likewise as in [9]. The dynamic C-arm projection data was created by forward projecting the 4D phantom according to the acquisition protocol. Poisson-distributed noise was added to the projections assuming an unattenuated X-ray density of $2.1 \cdot 10^5$ photons per mm^2 at the detector. The CBF maps were calculated from the reconstructed TACs using a standard deconvolution-based approach [11]. In this study we compared simple FDK reconstruction with the FDK-JBF, DIR-JBF, and DIR-MAP approaches with the parameters shown in Table I. We computed the RMSE and Pearson correlation (PC) of the resulting CBF maps to reference maps created from ground truth data using an automated ROI analysis [1]. Each of the 18 slices with stroke annotation of the CBF volume was divided into quadratic ROIs of size 8×8 mm^2 and the mean of each ROI was considered as a measurement for RMSE and PC computation. ROIs including voxels outside the brain or vessels were ignored. The slow C-arm rotation speed also leads to artifacts around arteries with high contrast dynamics if FBP-type reconstruction algorithms are used [12]. A qualitative comparison of DIR to FDK reconstruction with respect to such artifacts was performed.

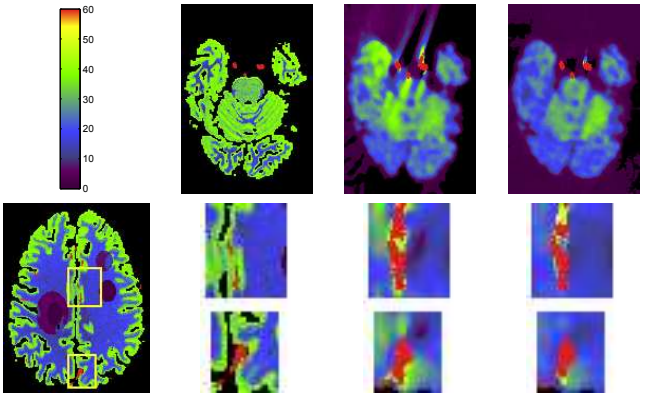

Reference FDK-JBF DIR-MAP

Figure 3. Artifacts in CBF maps (units: ml/100 g/min) comparing DIR-MAP and FDK-JBF reconstructions to the reference for two different slices. In the second row, zoomed views of the CBF maps shown in Figure 4 are provided as indicated by the rectangular regions in the lower left image.

	FDK	FDK-JBF	DIR-JBF	DIR-MAP
RMSE	8.4	4.6	6.2	3.7
PC (n =1815)	0.85	0.87	0.90	0.92

Table II
QUANTITATIVE RESULTS OF CBF MAPS FROM DIGITAL BRAIN PERFUSION PHANTOM DATA RECONSTRUCTED WITH DIFFERENT APPROACHES (RMSE: ROOT MEAN SQUARE ERROR IN [ML/100 ML/MIN], PC: PEARSON CORRELATION TO REFERENCE MAPS WITH SAMPLE SIZE N).

IV. RESULTS

Figure 4 shows the resulting CBF maps reconstructed with the different approaches. The quantitative results are shown in Table II. Figure 3 shows the artifacts around high contrast

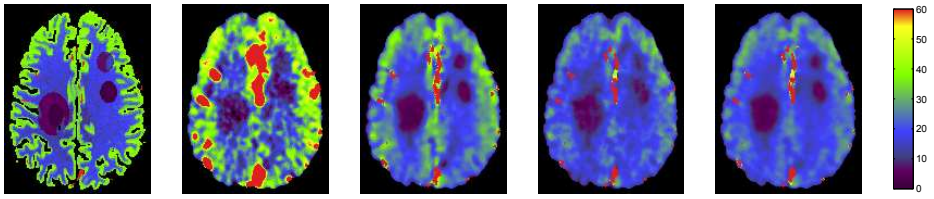

Figure 4. CBF maps (units: ml/100 ml/min) from digital brain perfusion phantom data reconstructed with different approaches.

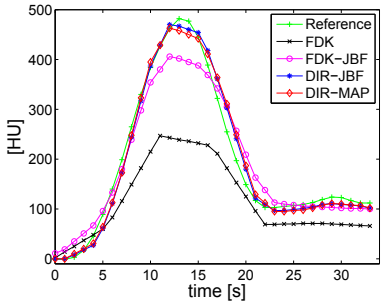

Figure 5. AIFs reconstructed with different approaches compared to ground truth AIF.

vessels in detail for the evaluated algorithms. Figure 5 shows the resulting arterial input functions (AIFs) of the discussed approaches. The reconstructions were performed on a laptop computer with an Intel i7 M 620 2×2.72 GHz CPU, 8 GB RAM, and an Nvidia Quadro FX 880M graphics chip set. The reconstruction of a typical 4D volume of size $256 \times 256 \times 86$ voxels and 14 spline weights per voxel took about 25 min using the DIR-MAP approach and about 1.5 min using the FDK approach, where the projection pre-processing and perfusion parameter computation is not included.

V. Discussion & Conclusions

The CBF maps in Figures 4 and 3 and the AIFs in Figure 5 show how the new DIR-MAP algorithm helps to improve the reconstructed blood flow maps and AIFs in comparison to the other evaluated techniques. The FDK maps have clearly the poorest quality: they are very noisy and the vessels are blurred into the soft tissue due to the very smooth reconstruction kernel. This also leads to a severe underestimation of the AIF and an overestimation of the perfusion values. Furthermore the stroke-affected areas are not well separated from the healthy tissue. The edge-preserving filter in the FDK-JBF reconstruction provides a highly improved noise level in the tissue without blurring the vessels. However, due to low C-arm rotation speed artifacts around high contrast vessels are visible and the AIF is still considerably underestimated. The DIR-JBF algorithm keenly reduces the FBP artifacts around the vessels by including the contrast dynamics into an iterative reconstruction approach and the temporal resolution of the reconstructed AIF is perceptibly improved. However, the resulting perfusion maps look more noisy. By including a statistical noise model, the new DIR-MAP compensates for this drawback. The DIR-MAP technique provides improved results with low noise level, reduced artifacts, improved AIF reconstruction, and physically correct perfusion values. This corresponds to the quantitative results in Table II. The DIR-MAP algorithm yields the best results of all algorithms. Comparing DIR-MAP to standard FDK reconstruction, the RMSE is reduced from 8.4 ml/100 ml/min to 3.7 ml/100 ml/min and PC is increased from 0.85 for standard FDK reconstruction to 0.92 on a sample size of $n = 1815$ ROIs.

In this work we extended our DIR-JBF algorithm [2] by including a statistical ray weighting to the DIR-MAP algorithm. We showed that the DIR-based algorithms help to increase the temporal resolution of the reconstructed TACs and provide an improved estimation of the AIF compared to FDK-type approaches. Furthermore the artifacts around vessels with high contrast are keenly reduced. However, we also found that the recently presented DIR-JBF algorithm produces more noisy perfusion maps than the FDK-JBF technique. By introducing a statistical ray weighting, we can compensate for this drawback.

References

[1] A. Fieselmann, A. Ganguly, Y. Deuerling-Zheng, M. Zellerhoff, C. Rohkohl, J. Boese, J. Hornegger, and R. Fahrig, "Interventional 4-D C-arm CT perfusion imaging using interleaved scanning and partial reconstruction interpolation," *IEEE Trans Med Imaging*, vol. 31, no. 4, pp. 892 – 906, 2012.

[2] M. Manhart, M. Kowarschik, A. Fieselmann, Y. Deuerling-Zheng, and J. Hornegger, "Fast dynamic reconstruction algorithm with joint bilateral filtering for perfusion C-arm CT," in *IEEE NSS MIC Conference Record*, Anaheim, USA, 2012, pp. 2304–2311.

[3] C. Neukirchen, M. Giordano, and S. Wiesner, "An iterative method for tomographic x-ray perfusion estimation in a decomposition model-based approach," *Medical Physics*, vol. 37, no. 12, pp. 6125–6141, 2010.

[4] J. Hsieh, "Adaptive filtering approach to the streaking artifact reduction due to X-ray photon starvation," *Medical Physics*, vol. 25, pp. 2139–2147, 1998.

[5] G. L. Zeng, *Medical Image Reconstruction*. Springer, 2009.

[6] K. Sauer and C. Bouman, "A local update strategy for iterative reconstruction from projections," *IEEE Trans. Signal Process.*, vol. 41, p. 1993, 534-548.

[7] M. Elad, "On the origin of the bilateral filter and ways to improve it," *IEEE Trans Img Proc*, vol. 11, pp. 1141–1151, 2002.

[8] A. J. Riordan, M. Prokop, M. A. Viergever, J. W. Dankbaar, E. J. Smit, and H. W. A. M. de Jong, "Validation of CT brain perfusion methods using a realistic dynamic head phantom," *Medical Physics*, vol. 38, no. 6, pp. 3212–3221, 2011.

[9] M. Manhart, A. Fieselmann, and Y. Deuerling-Zheng, "Evaluation of a tight frame reconstruction algorithm for perfusion C-arm CT using a realistic dynamic brain phantom," in *Proc. 2nd CT Meeting*, Salt Lake City, USA, 2012, pp. 123–126.

[10] Digital brain perfusion phantom. http://www5.cs.fau.de/data/.

[11] A. Fieselmann, M. Kowarschik, A. Ganguly, J. Hornegger, and R. Fahrig, "Deconvolution-based CT and MR brain perfusion measurement: Theoretical model revisited and practical implementation details," International Journal of Biomedical Imaging, 2011, article ID 467563.

[12] A. Fieselmann, F. Dennerlein, Y. Deuerling-Zheng, J. Boese, R. Fahrig, and J. Hornegger, "A model for filtered backprojection reconstruction artifacts due to time-varying attenuation values in perfusion C-arm CT," *Physics in Medicine and Biology*, vol. 56, no. 12, pp. 3701–3717, 2011.